Verification of Stress Transformation in Anisotropic Material Additively Manufactured by Fused Deposition Modeling (FDM)

M. Hossein Sehhat (hsehhat@mst.edu)

Department of Mechanical and Aerospace Engineering, Missouri University of Science and Technology, Rolla, MO 65409 https://orcid.org/0000-0002-7013-1642

Ali Mahdianikhotbesara

School of Mechanical Engineering, College of Engineering, University of Tehran, P.O. Box 11155/4563, Tehran, Iran https://orcid.org/0000-0002-9533-3259

Farzad Yadegari

Department of Mechanical Engineering, Amirkabir University of Technology (Tehran Polytechnic), Tehran, P.O.B. a15875-4413, Tehran, Iran

Research Article

Keywords: Fused Deposition Modeling (FDM), Anisotropic, Stress Transformation, Mechanical Properties, Design of Experiments (DOE), Additive Manufacturing

Posted Date: November 23rd, 2021

DOI: https://doi.org/10.21203/rs.3.rs-1107949/v1

Abstract

The widespread use of Additive Manufacturing (AM) has been extensively progressed in the past decade due to the convenience provided by AM in rapid and reliable part production. Fused Deposition Modeling (FDM) has witnessed even faster growth of application as its equipment is environmentally-friendly and easily adaptable. This increased use of FDM to manufacture prototypes and finished parts is accompanied by concerns that 3D printed parts do not perform the same as relatively homogeneous parts produced by molding or machining. As the interface between two faces of bonded material may be modeled by stress elements, in theory by modeling 3D printed layers subjected to tension at varying angles as transformed stress elements, the stress required to break the layer bonds can be determined. To evaluate such a relationship, in this study, the stresses calculated from stress transformation were compared with the behavior of 3D printed specimens subjected to tensile loads.

1. Introduction

Additive Manufacturing (AM) has improved the traditional method of part production through elimination of several inner-process manufacturing steps [1][2]. The layer-by-layer production fashion of AM can fabricate parts with complicated geometries in a single-step process [3][4]. The ease of manufacture of components produced by Fused Deposition Modeling (FDM) out of Polymers make them useful for rapid prototyping and scale testing of mechanisms and structures prior to mass-production or large-scale installation [5]. In addition, considering the process impacts on both user-safety and the environment, the filament format of feedstock material to FDM process is less hazardous than the other formats of feedstock, such as powder in powder-based AM processes [6][7]. Prior to the advent of affordable FDM technology, prototypes may have been manufactured out of polymers using injection molding, which is both time-consuming and expensive on smaller scales [8][9]. FDM allows parts with complex geometries to be rapidly manufactured cheaply, allowing designers to demonstrate and test the functionality of certain arrangements of parts [10].

There is debate, however, as to the suitability of objects made using FDM as accurate representations of their production counterparts, in the realm of either AM or traditional manufacturing processes [11][12] [13][14]. As FDM necessitates forming polymer filament into layers, the mechanical behavior under loading of the object at the layer boundaries may differ from the bulk behavior of the polymer that the part is composed of, making the part's loading behavior anisotropic [15][16]. While many manufacturers provide mechanical properties in the material specifications for their filament materials, the extensiveness of the documentation varies greatly in the tests performed and the print settings specified. For instance, while some filament manufacturers list filament's mechanical properties without mentioning the test standards or print settings, other manufacturers provide extensive documentation on test methods and print settings. Due to the planar nature of FDM, these documentations are still of limited use, as the relationship between the mechanical properties and the layer orientation is unclear. A mathematical model is required for determining such relationship; the simplest representation can be the transformation of a stress element.

Experimentation has already been performed in the literature to determine the stress-strain behavior and tensile strength of parts manufactured by FDM under certain loading cases. However, only the extreme layer orientation angles were investigated. In this study, through examining the mechanical properties of parts fabricated with FDM at different layer orientations, the stress transformations were used to derive a stress-angle curve.

2. Materials And Methods

Stress transformations

An element of the 3D printed material at the layer interface may be represented by a 3D stress element, and as the stress on the surface of the part σ_z may be neglected [17], it may instead be represented as a plane stress element as shown in Figure 1a. When subjected to loads at varying layer orientations, the stress element at the layer interface may be represented by a transformed stress element as shown in Figure 1b, with the forces acting on the stress element represented by the free-body-diagram (FBD) in Figure 1c.

As the test samples are considered to be in pure tension, σ_x and τ_{xy} may also be neglected, leaving the stresses at the layer interface dependent on only the tensile stress σ_y and layer orientation θ in Equations 1 through 3.

$$\sigma_{x'} = \frac{\sigma_y}{2} - \frac{\sigma_y}{2}\cos 2\theta \quad (1)$$

$$\sigma_{y'} = \frac{\sigma_y}{2} + \frac{\sigma_y}{2}\cos 2\theta \quad (2)$$

$$\tau_{x'y'} = \frac{\sigma_y}{2}\sin 2\theta \quad (3)$$

The stress transformation approach may be validated by comparing the maximum tensile stress developed at θ = 90° (tension normal to layers) to the transformed stress σ_{x1} developed at the layer interface for all other layer orientations. The validity of stress transformation will be verified if σ_y at θ = 90° is equal to the transformed stress σ_{x1} normal to the layer for all layer orientations tested.

Experimental Procedure

Tensile tests were performed on specimens modeled and tested according to the specifications from ASTM D638 [18][19]. Three test specimens per orientation were fabricated to evaluate the results' repeatability. All test specimens were produced from 1.75 mm diameter PETG filament using an Anet A8 3D printer with the following printing parameters: 240°C printing temperature, 60°C heated bed temperature, 40 mm/s print speed, 1.2mm layer thickness, 100% infill density, and concentric infill pattern. The test specimens were produced with printed material layers oriented from 0° to 90° in 15° increments, measured from normal to the direction of tension. Tensile tests were performed with an Instron 3365 tensile testing apparatus. The specimens were affixed between the grips of the tensile testing machine with a distance of 115 mm between the grips as specified in the ASTM D638, and they were tested under motion rate 3 mm/s.

3. Results And Discussion

Unlike most polymers, which usually experience a large amount of yield and elongation before breaking, most samples tested under the specified parameters of this study displayed a brittle fracture. show the various stress-strain profiles of all of the test samples, grouped by the angle between the layer plane and the load, in figures 11a through 12e. While the loads of each sample's failure were approximately equal, the extension of the sample only reached just above 2.25 mm before failure, while the other two managed to extend to 3.5 mm and 3.75 mm. Because the load at failure is the only variable being analyzed, this does not imply that Trial 1 at 75° is an outlier.

Trial 2's specimen at 60° failed at approximately half of the load and extension necessary to rupture the other two trials. This load was therefore considered an outlier, and was not considered in calculations. The behavior of the specimen in Trial 3 at 0° in Figure 3 was particularly noteworthy, because instead of undergoing brittle fracture upon failure, it experienced ductile yielding with an elongation of over 28 mm, and still did not experience complete separation. While its failure behavior was inconsistent with those of other specimens, the failure load was consistent with the other specimens of the set, and thus the strength of this particular sample was considered during calculation.

After obtaining the ultimate strengths of the samples at each layer angle, each set of ultimate strengths was averaged and plotted against the layer Angle relative to the load in Figure 4.

Changing the angle reference from "relative to load" to "relative to the horizontal" axis for later use in the stress transformation equations, these loads were used to find the tensile stresses, and both were plotted in Figure 5.

Using Equation 1 to find the transformed stress $\sigma_{x'}$ normal to the layer interface and plotting against the layer interface angle in Figure 6 revealed that the stress was not constant at any regions.

The remaining stresses $\sigma_{y'}$ and $\tau_{x'y'}$ were calculated and plotted with $\sigma_{x'}$ in Figure 7.

Realizing that rather than experiencing a single stress the layers were experiencing combined loading, the maximum principal stress for each layer angle was calculated using Equation 4 and plotted in Figure 8.

$$\tau_{x'y'} = \frac{\sigma_y}{2} \sin 2\theta \qquad (4)$$

This revealed that the maximum principal stress was the constant stress between all test specimens at around 38 MPa, with the exception of the samples tested with layers printed at 75°to the load, which consistently failed at much lower stresses.

4. Conclusion

In this study, Fused Deposition Modeling (FDM) Additive Manufacturing (AM) was used to fabricate parts with different layer orientations. Through examining the mechanical properties of fabricated parts, the stress transformations were used to generate a stress-angle curve. The stresses calculated from stress transformation were compared with the behavior of 3D printed specimens subjected to tensile loads. Based on the results, the initial hypothesis, that the transformation of a stress element could be validated if the calculated transformed stress $\sigma_{x'}$ normal to the layer interface resulting from tensile tests was constant, was disproven. However, this was the result of failure to consider the other stresses acting at the layer interface rather than a fault in the principles of stress transformation, as the maximum principal stress resulting from the combined calculated transformed stresses relative to the layer angle was constant, regardless of whether the specimen experienced failure at the layer interface or within the layer material. The notable exceptions to this were the specimens with layers 75° relative to the load. Noting the more pronounced striations along the samples used in the 75° tests, it is possible that an environmental factor during printing, such as temperature or humidity change, may have been responsible for the degradation of the samples' structural integrity, causing them to fail at much lower stresses.

References

1. M.H. Sehhat, A. Mahdianikhotbesara, M. Hadad, Formability Investigation for Perforated Steel Sheets, SAE MobilityRxiv, (2021). https://doi.org/10.47953/SAE-PP-00182.
2. A. Mahdianikhotbesara, M.H. Sehhat, M. Hadad, Experimental Study on Micro-Friction Stir Welding of Dissimilar Butt Joints Between Al 1050 and Pure Copper, Metallogr. Microstruct. Anal. 2021. (2021) 1–16. https://doi.org/10.1007/S13632-021-00771-5.
3. M.H. Sehhat, B. Behdani, C. Hung, H. Ali, Development of an Empirical Model on Melt Pool Variation in Laser Foil Printing Additive Manufacturing Process Using Statistical Analysis, (2021).
4. C.H. Hung, W.T. Chen, M.H. Sehhat, M.C. Leu, The effect of laser welding modes on mechanical properties and microstructure of 304L stainless steel parts fabricated by laser-foil-printing additive

manufacturing, Int. J. Adv. Manuf. Technol. (2020) 1–11. https://doi.org/10.1007/s00170-020-06402-7.

5. B. Behdani, M. Senter, L. Mason, M. Leu, J. Park, Numerical Study on the Temperature-Dependent Viscosity Effect on the Strand Shape in Extrusion-Based Additive Manufacturing, J. Manuf. Mater. Process. 4 (2020) 46. https://doi.org/10.3390/jmmp4020046.
6. M.H. Sehhat, · Ali Mahdianikhotbesara, Powder spreading in laser-powder bed fusion process, Granul. Matter. 23, 89 (2021). https://doi.org/10.1007/s10035-021-01162-x.
7. M.H. Sehhat, A.T. Sutton, C.H. Hung, J.W. Newkirk, M.C. Leu, Investigation of Mechanical Properties of Parts Fabricated with Gas- and Water-Atomized 304L Stainless Steel Powder in the Laser Powder Bed Fusion Process, JOM, (2021) 1–10. https://doi.org/10.1007/s11837-021-05029-7.
8. A.-C. Liou, R.-H. Chen, Injection molding of polymer micro-and sub-micron structures with high-aspect ratios, Int J Adv Manuf Technol. 28 (2006) 1097–1103. https://doi.org/10.1007/s00170-004-2455-2.
9. Y.C. Su, J. Shah, L. Lin, Implementation and analysis of polymeric microstructure replication by micro injection molding, J. Micromechanics Microengineering. 14 (2003) 415. https://doi.org/10.1088/0960-1317/14/3/015.
10. C. Esposito Corcione, F. Gervaso, F. Scalera, F. Montagna, A. Sannino, A. Maffezzoli, The feasibility of printing polylactic acid–nanohydroxyapatite composites using a low-cost fused deposition modeling 3D printer, J. Appl. Polym. Sci. 134 (2017) 44656. https://doi.org/10.1002/APP.44656.
11. P.D. Nezhadfar, S. Thompson, A. Saharan, N. Phan, N. Shamsaei, Fatigue and Failure Analysis of an Additively Manufactured Contemporary Aluminum Alloy, in: Miner. Met. Mater. Ser., Springer Science and Business Media Deutschland GmbH, 2021: pp. 212–219. https://doi.org/10.1007/978-3-030-65396-5_31.
12. P.D. Nezhadfar, A. Soltani-Tehrani, N. Shamsaei, Effect of Preheating Build Platform on Microstructure and Mechanical Properties of Additively Manufactured 316L Stainless Steel, (n.d.).
13. A.P. Jirandehi, T.N. Chakherlou, A fatigue crack initiation and growth life estimation method in single-bolted connections, J. Strain Anal. Eng. Des. 54 (2019) 79–94. https://doi.org/10.1177/0309324719829274.
14. H. Ghadimi, A.P. Jirandehi, S. Nemati, S. Guo, Small-sized specimen design with the provision for high-frequency bending-fatigue testing, Fatigue Fract. Eng. Mater. Struct. (2021). https://doi.org/10.1111/FFE.13589.
15. M.H. Sehhat, A. Mahdianikhotbesara, F. Yadegari, Impact of Temperature and Material Variation on Mechanical Properties of Parts Fabricated with Fused Deposition Modelling (FDM) Additive Manufacturing, (2021). https://doi.org/10.21203/RS.3.RS-1079840/V1.
16. C. Ziemian, M. Sharma, S. Ziemian, 7 Anisotropic Mechanical Properties of ABS Parts Fabricated by Fused Deposition Modelling, (n.d.).
17. Mechanics of Materials: Stress Transformation » Mechanics of Slender Structures | Boston University, (n.d.). https://www.bu.edu/moss/mechanics-of-materials-stress-transformation/ (accessed November 19, 2021).

18. ASTM D638 - 14 Standard Test Method for Tensile Properties of Plastics, (n.d.). https://www.astm.org/Standards/D638 (accessed November 12, 2021).
19. A. Lanzotti, M. Grasso, G. Staiano, M. Martorelli, The impact of process parameters on mechanical properties of parts fabricated in PLA with an open-source 3-D printer, Rapid Prototyp. J. 21 (2015) 604–617. https://doi.org/10.1108/RPJ-09-2014-0135/FULL/XML.

Declarations

Competing interests: The authors declare no competing interests.

Figures

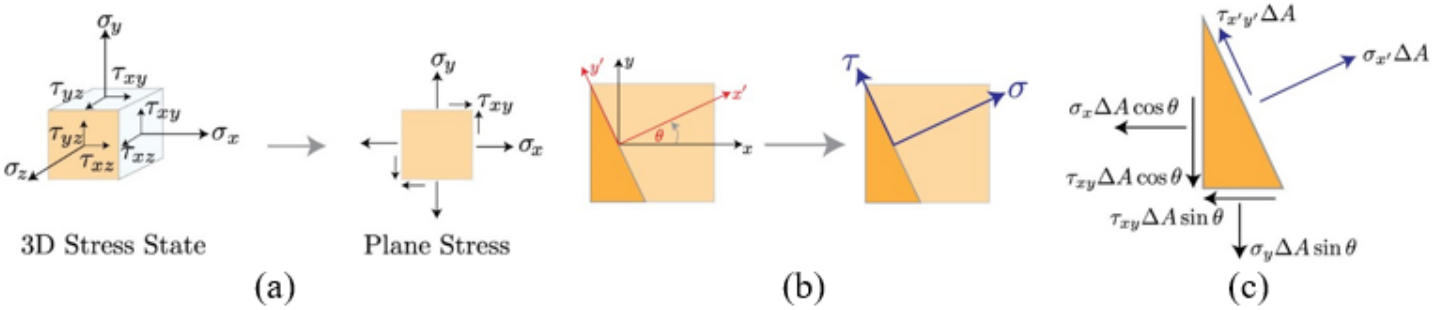

Figure 1

(a) 3D and Plane Stress Element, (b) Stress Transformation of Plane Stress Element, (c) Transformed Stress Element FBD.

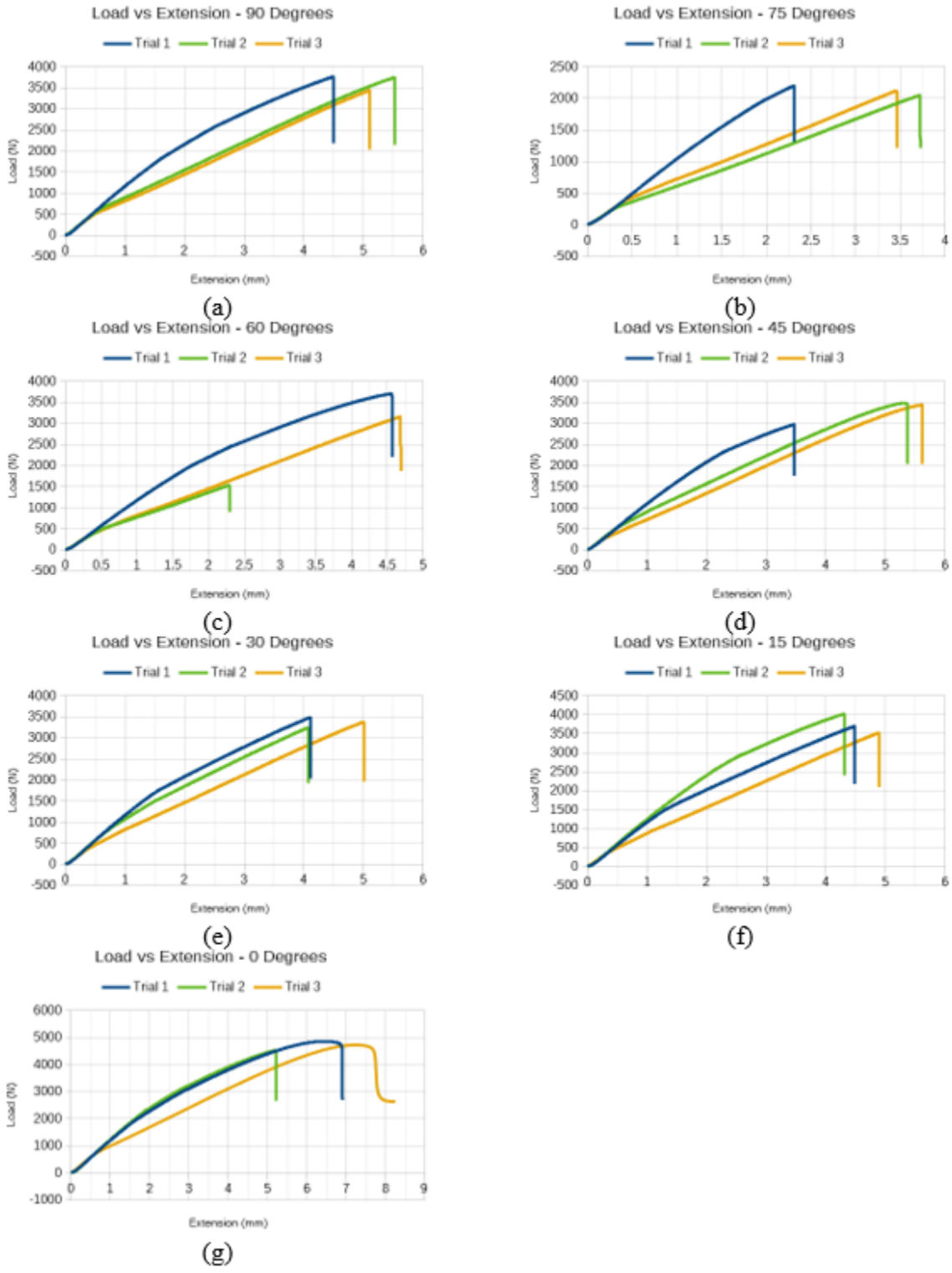

Figure 2

Stress-Strain curves obtained from samples with layers (a) perpendicular to the load, (b) 75°, 60°, 45°, 30°, 15°, and parallel to the load.

Figure 3

Ductile failure of sample 3 taken at 0°.

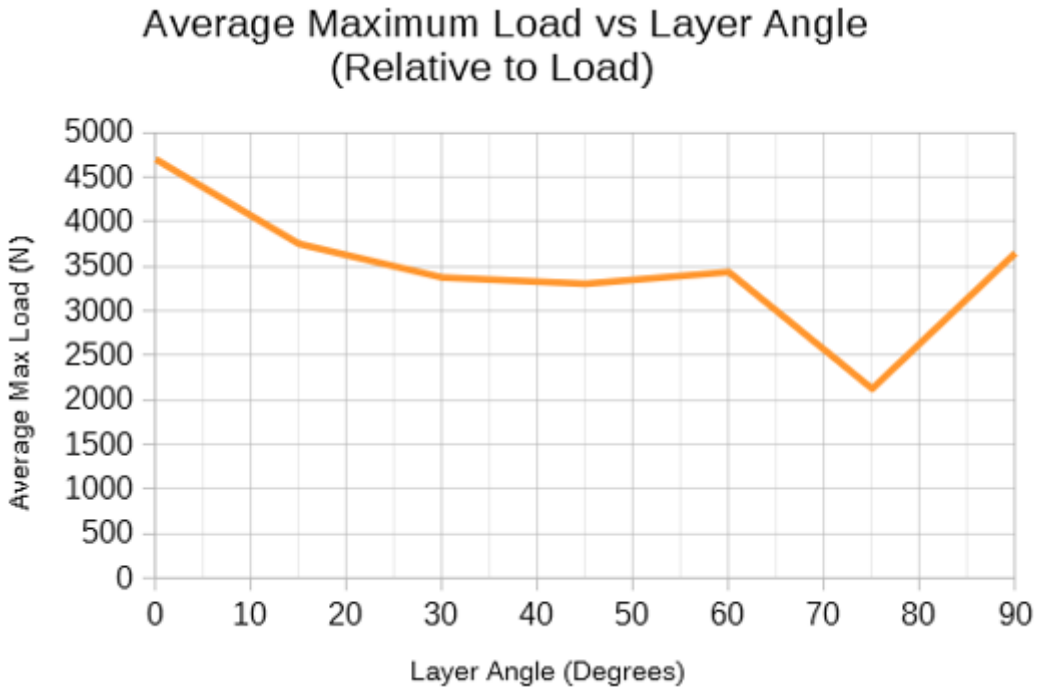

Figure 4

Average Maximum Stress vs Layer Angle.

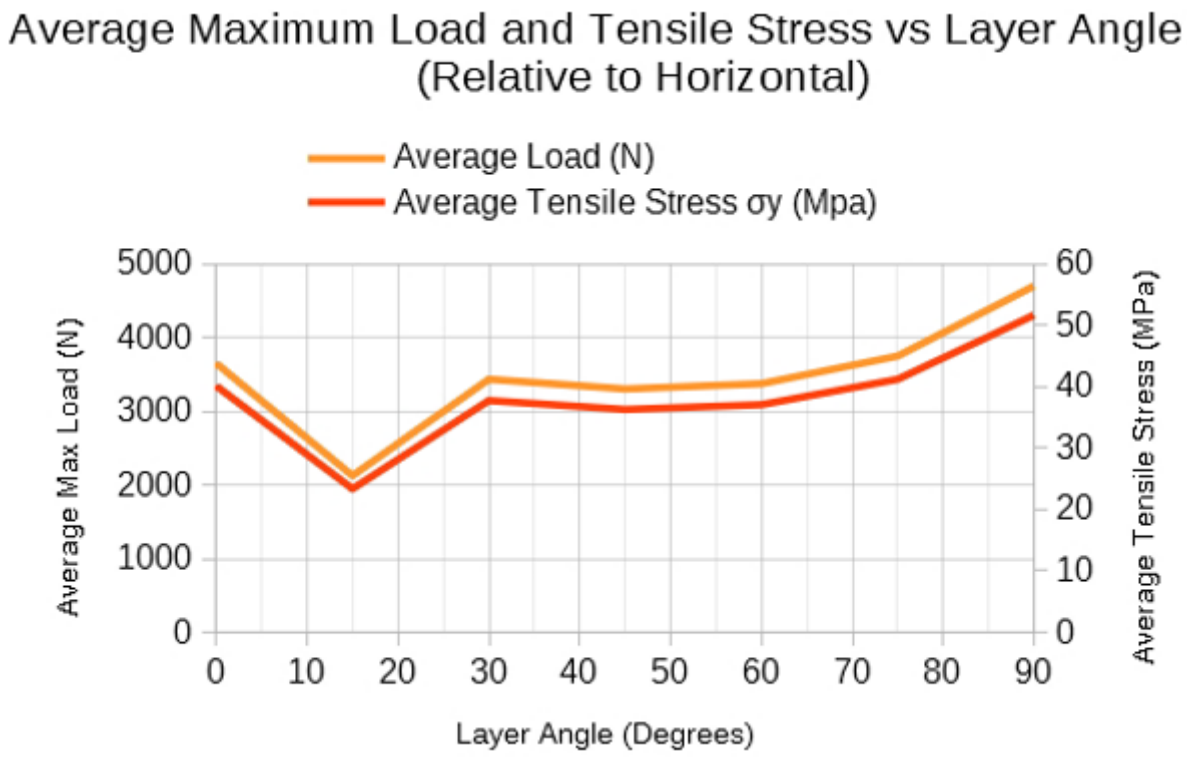

Figure 5

Specimen Failure Load and Tensile Stress vs Layer Angle.

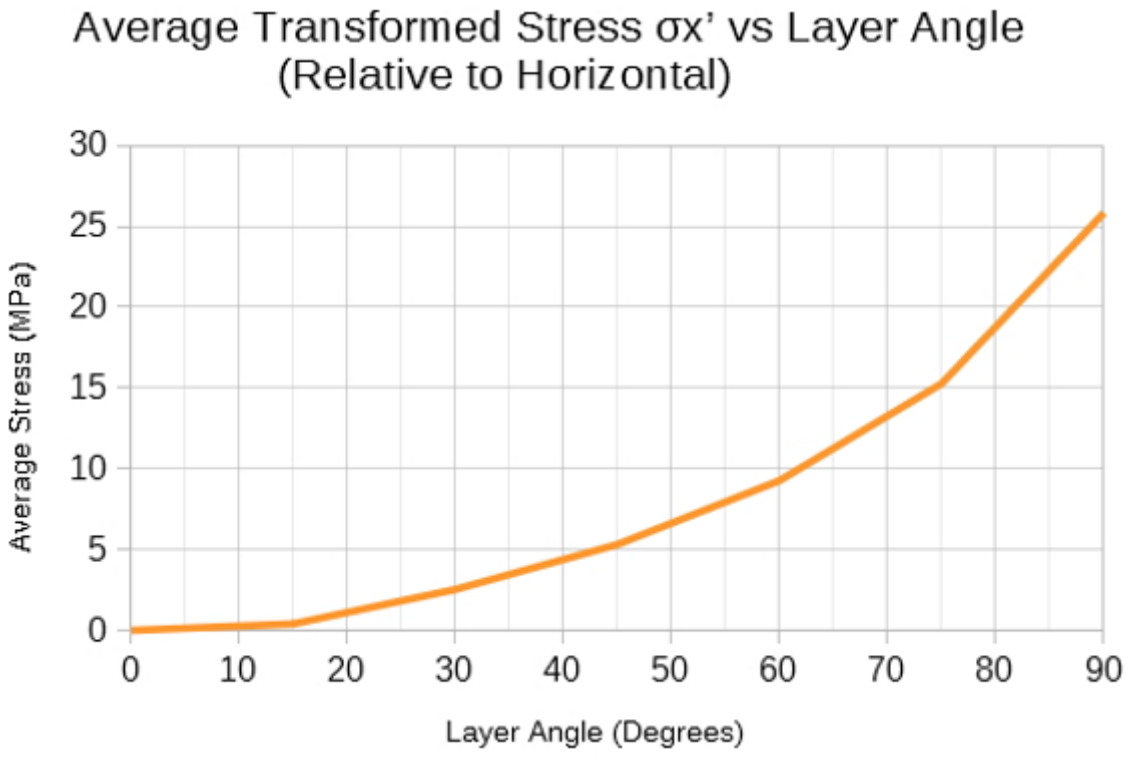

Figure 6

Transformed Normal Stress vs Layer Angle.

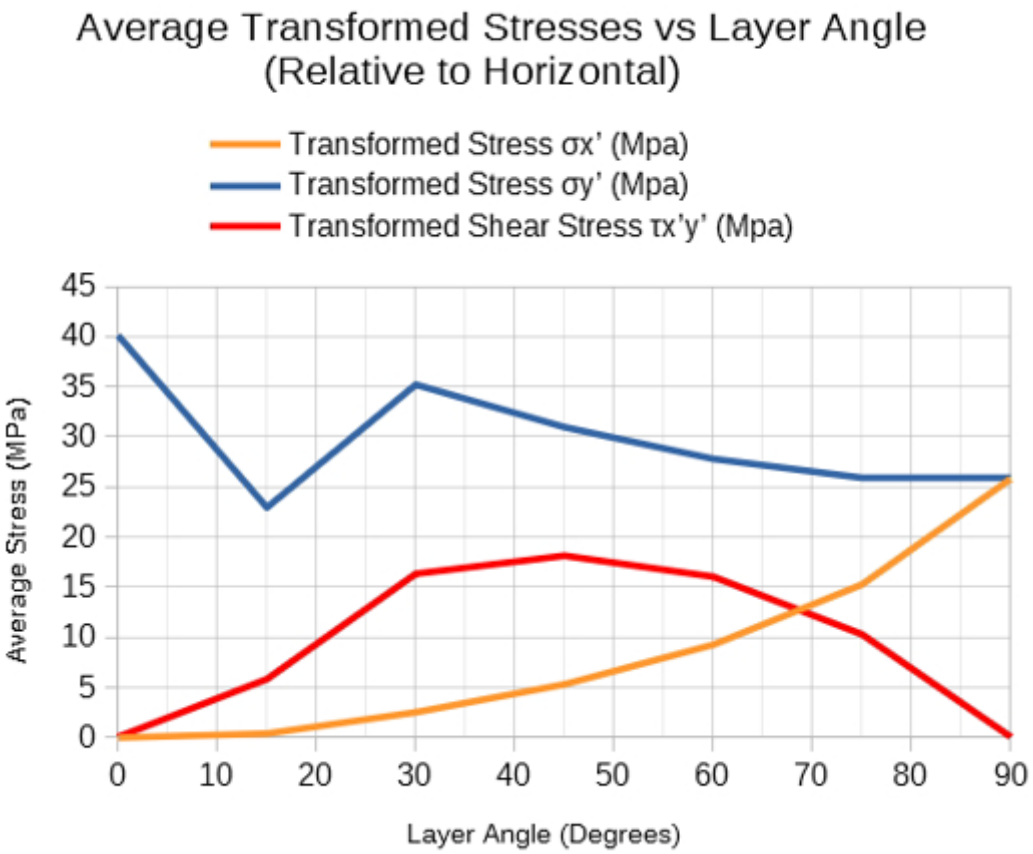

Figure 7

Transformed Stresses vs Layer Angle.

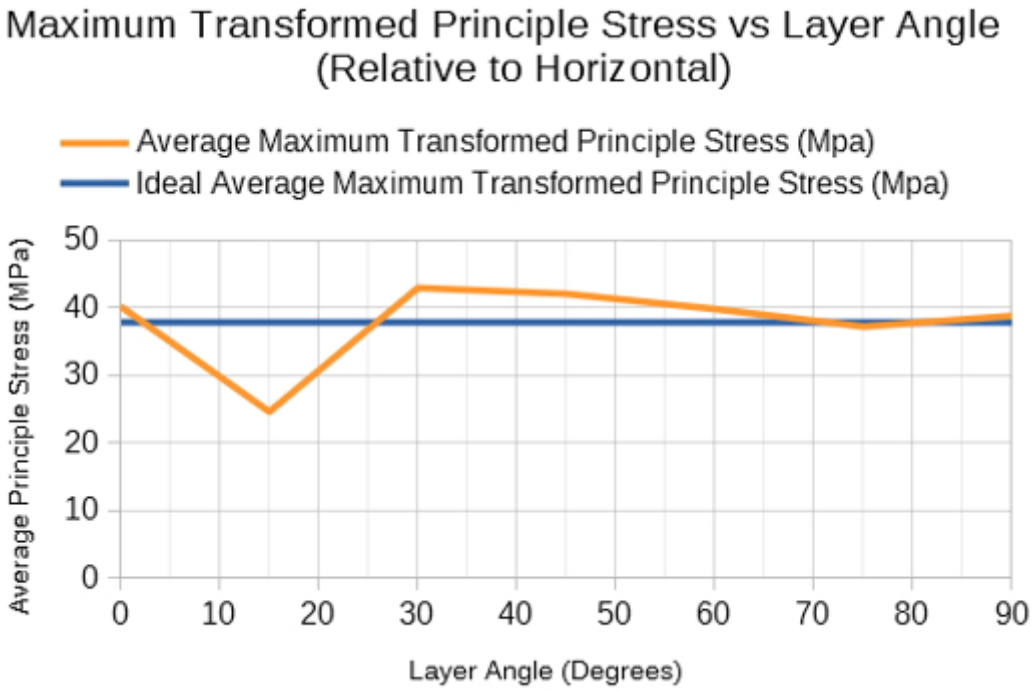

Figure 8

Transformed Principal Stress vs Layer Angle.